

Electrochemical Functionalization as a Promising Avenue for Glucose Oxidase Immobilization at Carbon Nanotubes: Enhanced Direct Electron Transfer Process

Mouna Moumene¹, Dominic Rochefort² and Mohamed Mohamedi^{1,}*

¹Institut National de la Recherche Scientifique (INRS)-Énergie, Matériaux et Télécommunications (EMT), 1650 Boulevard Lionel Boulet, Varennes, Québec, J3X 1S2, Canada.

²Département de Chimie, Université de Montréal, CP 6128 Centre-Ville, Montréal Québec, H3C 3J7, Canada

*E-mail: mohamedi@emt.inrs.ca

Received: 2 December 2012 / *Accepted:* 23 December 2012 / *Published:* 1 February 2013

This work demonstrates an approach for building bioelectrocatalytic interfaces by electrochemically functionalizing carbon nanotubes surface to create a conductive matrix for immobilization of enzymes. Such a strategy not only is simple but presents an opportunity to intimately interface an enzyme and manifests direct electron transfer features. Electrochemically functionalized carbon nanotubes (CNT_{EF})-glucose oxidase (GOx) electrodes are evaluated electrochemically and characterized by means of FESEM and X-ray photoelectron spectroscopy (XPS). The immobilization of GOx on the CNTs surface was confirmed with XPS analysis. Square wave voltammetry of the CNT_{EF}-GOx in argon saturated PBS solution (pH 7.2) displayed a net current peak at a potential close to that of the FAD/FADH₂ cofactor of immobilized GOx. In the presence of glucose, the immobilized GOx demonstrated its ability to simultaneously undergo DET with the electrode and retains biocatalytic activity up to 10 mM of glucose concentration. The proposed electrochemical functionalization method could be without doubt extended to immobilize and evaluate the direct electron transfer of other redox enzymes or proteins on carbon nanostructures.

Keywords: Carbon nanotubes; glucose-oxidase; electrochemical functionalization; enzyme immobilization; direct electron transfer

1. INTRODUCTION

Several biodevices utilize redox enzymes as biocatalysts. The redox enzymes, which are separated and purified from an organism, participate in the electron transfer chain that occurs between the substrate and the anode and the cathode. However, redox enzymes are incapable of achieving an

efficient direct contact with the electrode since their redox centers are insulated from the conductive support by the protein matrices. To facilitate the electrons exchange between these enzymes with the electrodes, mediators, which are dependent on the class of oxidoreductase enzymes, are utilized. This naturally adds significant cost, intricacy to the system and declines the current density of the electrode.

Critical challenges in the successful development of a practically valuable mediatorless enzyme electrodes for biomedical devices such as biofuel cells and biosensors is an efficient immobilization on the electrode and an effective electrical communication between the enzyme molecule and the electrode surface using direct electron transfer. For more details regarding glucose based biosensors and biofuel cells the reader is directed to the reviews of Rad [1] and Meredith [2], respectively.

The glucose oxidase (GOx) enzymes catalyze glucose oxidation at very low electrochemical potentials, making them attractive protein biocatalysts anodes [3-5]. Direct electron transfer (DET) mode with enzymatic electrodes therefore eliminates the inherent limitations of redox mediators in bioelectrocatalytic applications [6]. In addition, immobilization methods using carbon nanotubes (CNTs) are an attractive means to create a 3-dimensional, porous, conductive catalytic matrix on an electrode surface [7]. Creating an approach that will reliably link the redox enzymes to well dispersed, conductive CNTs may advance bioelectrocatalysis. Imaginative methodologies such as linking multicopper oxidases (MCO) to CNTs via molecular tethering reagent, displayed high bioelectrocatalytic activity for oxygen reduction [8], or CNT/Nafion-based electrodes for immobilizing enzyme [9], graphene-based bioelectrodes [10], enzyme immobilized onto reduced graphene oxide/ZnO composite [11] are highly encouraging.

Functionalization that consists into the modification or transformation of CNTs surface may be a promising approach for the immobilization of enzymes. A first goal of the functionalization is to anchor chemical species (in this case, enzymes) on the surface of CNTs using an appropriate treatment. In many situations, the treatment is oxidative which yield to the creation of defects of surfaces. The creation of these surface defects is important for electrocatalytic applications because the electroactivity at the CNT edge planes is greater than the basal planes [12]. In other words, CNTs subjected to oxidative treatments bear many oxygenated moieties, such as quinine-like groups at the end and defects in the sidewall. Most of those moieties are electrochemically redox active and could be used to accelerate the electron transfer kinetics of enzyme species; they thereby constitute another source of the electrocatalytic activities observed for pristine CNTs themselves.

Our interest in the study of the functionalization of CNTs supports is oriented towards development of mediatorless Enzymatic Biofuel Cell (EBFC) electrodes. EBFCs are potential power sources for external portable electronics and for implantable medical devices such as pacemakers and sensors. An overview of recent advances and applications of BFCs can be found elsewhere [13-15]. Briefly, EBFC works using glucose and dissolved oxygen as fuel and oxidant, respectively. Using the appropriate redox enzymes as biocatalysts, electricity is produced by the biocatalytic oxidation of glucose at the anode, coupled with the reduction of dissolved oxygen at the cathode. This work addresses some of our efforts into developing efficient enzyme immobilization via electrochemical approaches for biofuel cells applications. The approach is based on the electrochemical functionalization of CNTs in mild acidic conditions. This procedure yields to several advantageous surface properties such as: (i) creation of surface defects that are highly electroactive, (ii) oxygen

functional groups which make the CNTs more hydrophilic and, (iii) the creation of large specific surface area with high porosity [16]. All these useful properties are expected to insure strong attachment of the enzyme and an enhanced DET. The electrochemical functionalization approach is applied here to Glucose oxidase (GOx) which is commonly used as an anode catalyst in EBFCs and as sensing electrode in glucose electrochemical sensors.

2. EXPERIMENTAL

2.1. Materials synthesis

CNTs were grown at 700°C by chemical vapor deposition (CVD) method using Ni as catalyst deposited by PLD onto a carbon paper (CP, Toray), acetylene (carbon source), hydrogen and argon (gas carrier) gases at flow rates of 20, 140 and 100 sccm, respectively. Full details regarding the CNTs synthesis can be found in our previous publications [17].

2.2. Characterization

The surface morphology of the as-prepared samples was examined by means of a field emission scanning electron microscope (SEM, JEOL, JSM 7401F apparatus).

X-ray Photoelectron Spectroscopy (XPS) was conducted for elemental composition of the material's surface and its chemical environment. The XPS study was performed with a VG Instruments Escalab 220i-XL surface microanalysis system equipped with hemispherical analyzer and Al K α X-ray source (1486.6 eV). Survey scans in the range 0–1000 eV were recorded at 100 eV pass energy with a step size of 1 eV. Core level spectra were obtained for C 1s and recorded at 20 eV pass energy with a step size of 0.1 eV. Curve fitting of the XPS data was carried out with casaXPS version 2.3.15. A semi-quantitative evaluation of relative atomic surface concentrations was obtained by considering their corresponding sensitivity factors: C1s (1.0), and O1s (2.93). The binding energies were corrected for surface charging by referencing them to the designated hydrocarbon C1s binding energy of 285.5 eV.

Micro-Raman spectroscopy was performed by using the 514.5 nm (2.41 eV) laser radiation of an Ar $^+$ laser with a circular polarization. The laser beam was focused onto the sample to a spot size of 1 μm in diameter (micro-Raman spectroscopy, Renishaw Imaging Microscope WireTM).

2.3. Electrochemical functionalization

The electrochemical functionalization consisted in electro-oxidizing the CNTs by potential cycling from 0.15 and 2 V (vs. Ag/AgCl reference electrode) in 0.2 M HNO₃ solution using cyclic voltammetry (CV). Usually, the functionalization time is about 18.5 min (15 CV cycles at 50 mV s⁻¹). The resulting electrochemically functionalized CNTs is denoted CNT_{EF}.

2.4. Preparation of the GOx-CNTs electrode

Glucose oxidase was immobilized on the substrates by physisorption. To do so, the CP-CNTs and CP-CNT_{EF} samples were soaked in phosphate buffer solution (PBS, pH=7.2, from Sigma-Aldrich, Canada Ltd.) containing 15mg/mL GOx from *Aspergillus niger* (168800 units/G Sigma-Aldrich Canada Ltd.) and stored overnight at 4 °C in a refrigerator before use.

2.5. Electrochemical measurements

Electron transfer properties of the as-prepared CNTs and CNT_{EF} were assessed by CV in a benchmark solution consisting of 1.0 mM potassium ferrocyanide and 1.0 M KCl solution.

DET properties between the GOx and the CNTs substrates were studied by CV and square-wave voltammetry (SWV) in a deaerated phosphate buffer solution (PBS, pH=7.2) with and without glucose solution (D-(+)-Glucose, ACS reagent grade, from Sigma-Aldrich).

All electrochemical measurements were conducted at room temperature using a three-electrode cell with the reference electrode and counter electrode being an Ag/AgCl, 3M NaCl and a platinum coil, respectively. Data were controlled and acquired with a potentiostat/galvanostat Autolab from EcoChemie.

3. RESULTS AND DISCUSSIONS

3.1. Characterisation

Figure 1a displays SEM images with increasing magnifications of as-grown CNTs on CP substrate which is also shown in the insert of Fig. 1a.

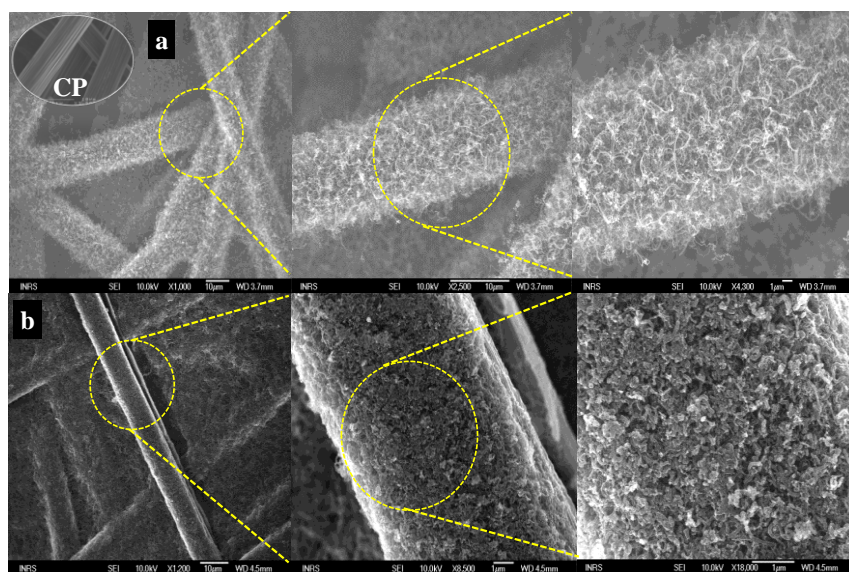


Figure 1. FESEM images with increasing magnification of: (a) CNTs synthesized on CP. Insert shows the bare CP before CNTs growth, and (b) electrochemically functionalized CNTs (CNT_{EF}).

It can be seen that the carbon microfibers are covered by packed wavy aligned arrays of fine CNTs with lengths greater than tens of micrometers. Figure 1b shows SEM images of CNTs that were subjected to electrochemical oxidation in 0.2 M HNO₃ solution. The images clearly reveal that the electrochemical oxidation process dramatically alters the surface morphology of the CNTs. Indeed, after the oxidation, the surface of the CNTs became heterogeneous due to acidic electrochemical etching, i.e., the CNTs are found to get much rougher and to shrink with a strong degree of coiling.

The effect of the electrochemical oxidation on the graphitic structure of the CNTs was further examined by micro Raman spectroscopy and the results are shown in Fig. 2. Typically, all spectra exhibit two main characteristic bands in the spectral region between 1000 and 2000 cm⁻¹ (D and G modes). The first order G mode (E_{2g} symmetry) at ~1601 cm⁻¹ is ascribed to a regular sp² graphitic network, while the D mode (A_{1g} symmetry) at ~1347 cm⁻¹ reflects the disorder and defects in the carbon lattice [18]. Generally, the intensities ratio between the D and G modes (I_D/I_G) can be used as an indicator of the crystallite and defect sites surface density [19]. The value of the intensity ratio observed in the pristine CNT ($I_D/I_G=0.82$) increases to 0.95 in the CNT_{EF}. This result indicates that the electrochemical oxidation enriched the surface of the CNTs with more structural defects at their surface.

It was also shown that the D band depended on the in-plane correlation length (L_a) or carbon grain size, a feature for which an empirical law was proposed in 1970 by Tuinstra and Koenig [19]: $I_D/I_G = C(\lambda)/L_a$ (nm) with $C(\lambda=514.5 \text{ nm}) = 4.4 \text{ nm}$. Using this equation, we found an L_a of 5.37 nm and 4.63 nm for pristine CNTs and CNT_{EF}, respectively. This decrease in L_a indicates that the atomic ordering or crystallinity of the CNTs was reduced because of the electrochemical oxidation.

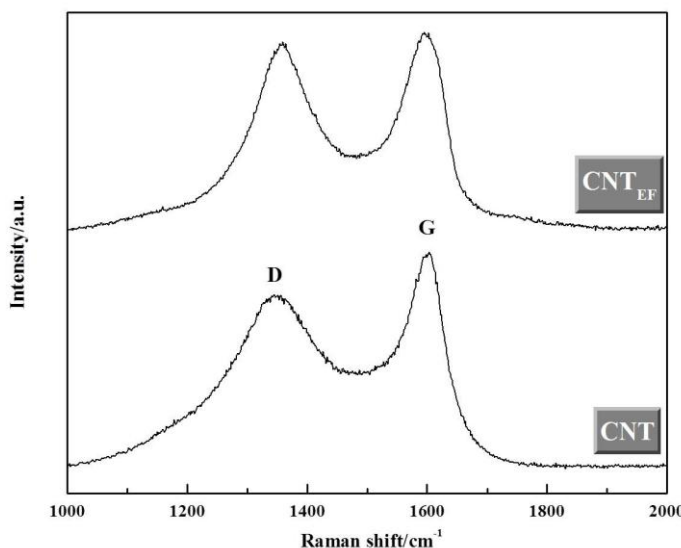


Figure 2. Micro-Raman spectra of the pristine CNTs and electrochemically functionalized CNTs (CNT_{EF}).

Next, XPS-measurements were carried out to obtain information about the chemical composition of the CNTs and CNT_{EF} and the binding characteristics of the elements at the surface. The

XPS wide survey profiles of pristine CNTs and CNT_{EF} are reported in Fig. 3 (top middle). Both samples contain only carbon and oxygen at their surfaces. The CNT XPS spectrum displays a C 1s core level peak located at a binding energy (BE) of 284.2~284.5 eV and a core level O 1s peak at $BE=532.2\sim532.5$ eV. The full width at half maximum (fwhm) of the carbon peak became wider from 1 to 1.47 eV in the electrochemical oxidation process indicating more disordering of the carbon lattice [20], which is line with the Raman findings.

The atomic concentration at the pristine CNTs surface is 94.8 at% and 5.20 at % of C and O, respectively. The presence of small amount oxygen occurred as a result of exposure to ambient air. On the other hand, at the CNT_{EF} surface, the concentration of C and O elements differs from those observed at pristine CNTs. Indeed, the atomic concentration of C and O is 70.10 at% and 29.90 at % of C and O, respectively. Thus, the relative ratios of the surface concentration of oxygen to carbon for CNT_{EF} is ~7.75 times higher than for pristine CNTs. It is thus clear that the electrochemical oxidation induced considerable increase in the concentration of oxygen at the surface of the CNTs.

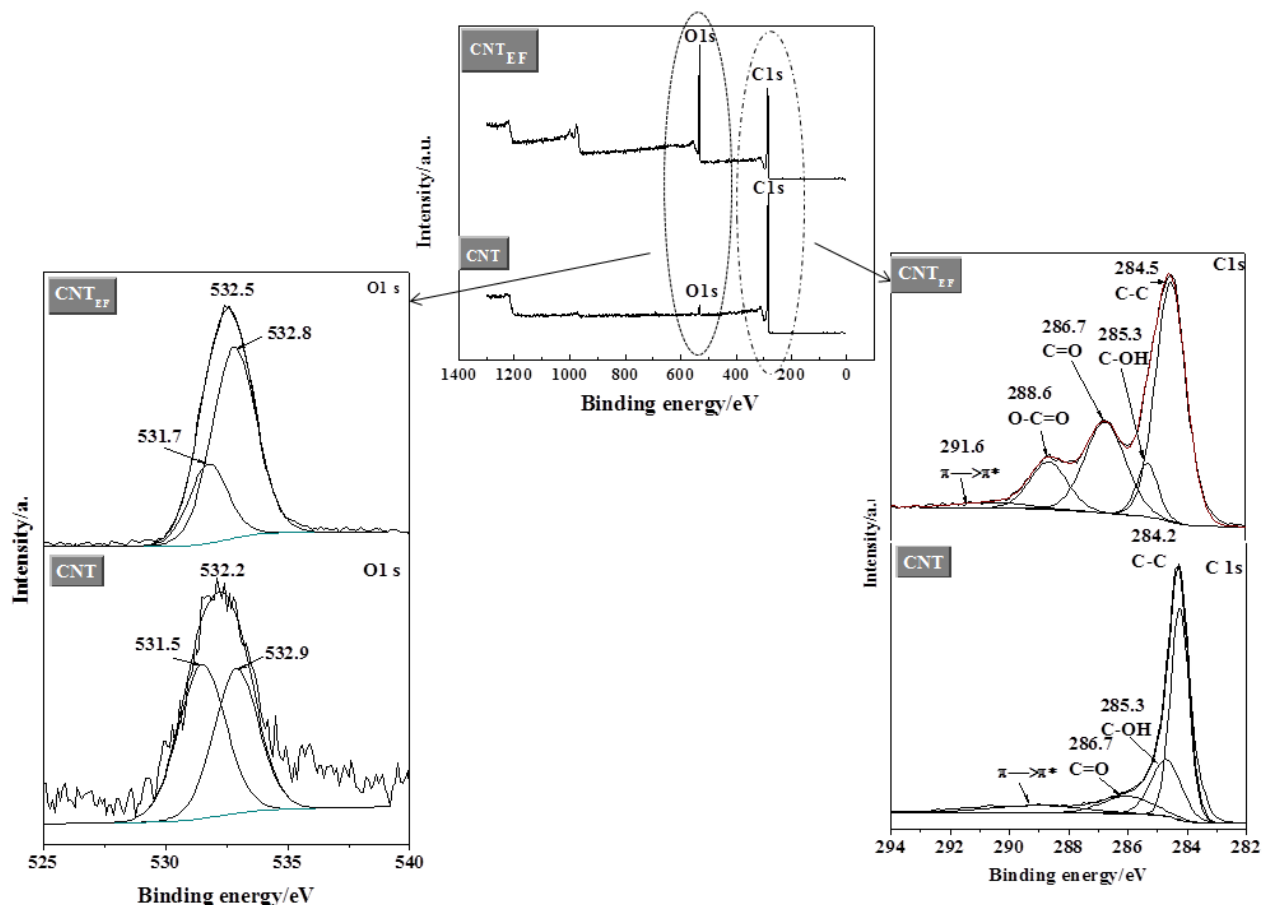


Figure 3. XPS analysis of CNTs and CNT_{EF} : (top centered) wide survey XPS spectra, (bottom right) high-resolution XPS C 1s core level spectra and (bottom left) high-resolution XPS O 1s core level spectra.

The high-resolution C1s core level peaks obtained for the pristine CNTs (Fig. 3, bottom right), could be fairly deconvoluted into three major components centered around 284.2, 285.3, and 286.7

attributed to C-C, C-OH and C=O functional groups, respectively. These values are in accordance with those found in the literature [21-22]. A fourth broad peak present at 291.6 eV is the shake-up line as a result of a shake-up process that induces the energy of the $\pi \rightarrow \pi^*$ transition. Similar binding energies were found for the CNT_{EF} sample (Fig. 3, bottom right), which were attributed to the same functional groups. An additional fitting peak at 288.6 eV is ascribable to O-C=O groups [21-22]. Figure 3 (bottom left) shows the O1s region spectra fitted to two peaks for CNT and CNT_{EF}. This region has been fitted in a way consistent with numerous prior studies of surface-treated carbon [23-24]. Accordingly, peaks appearing within 531.5~531.7, and 532.8~532.9 eV assigned to O-C and C=O groups, respectively.

3.2. Electron transfer properties of CP-CNT and CP-CNT_{EF}

The oxidation of potassium ferrocyanide serves as a benchmark in investigating electrochemistry at different carbon and metallic electrodes [25-27]. The electrochemical oxidation generates ferricyanide, and the analysis of the redox couple $[\text{Fe}(\text{CN})^{4-}]_6/[\text{Fe}(\text{CN})^{3-}]_6$ kinetics provide information about the electron transfer kinetics and the electroactive surface area (ESA) of the electrode. Figures 4a and 4b show the resulting CVs respectively, for the pristine CNTs and CNT_{EF} electrodes in 1.0 mM potassium ferrocyanide, over a range of different scan rates (5-200 mV s⁻¹). At both electrodes the $[\text{Fe}(\text{CN})^{4-}]_6/[\text{Fe}(\text{CN})^{3-}]_6$ redox pairs are well-defined. In addition, the CVs of the CNT_{EF} display a large capacitive current. This capacitive current indicates that CNT_{EF} possess surface area higher than pristine CNTs. The anodic peak current (I_{pA}) corrected from the capacitive current was found to vary linearly with the square root of the potential scan rate (Fig. 4c) indicating that the charge transfer is under diffusion control [28]. From the electrocatalytic activity point of view, the CNT_{EF} shows peak current densities much larger than those at the CNTs electrode. At a scan rate of 5 mV s⁻¹ (quasi steady-state conditions), the anodic peak-to-cathodic peak separation is ~82 mV and 49 mV at the CNTs and CNT_{EF}, respectively. For a one-electron electrochemically reversible system, the ideal peak-to-peak separation at 298 K is 59 mV [28-29].

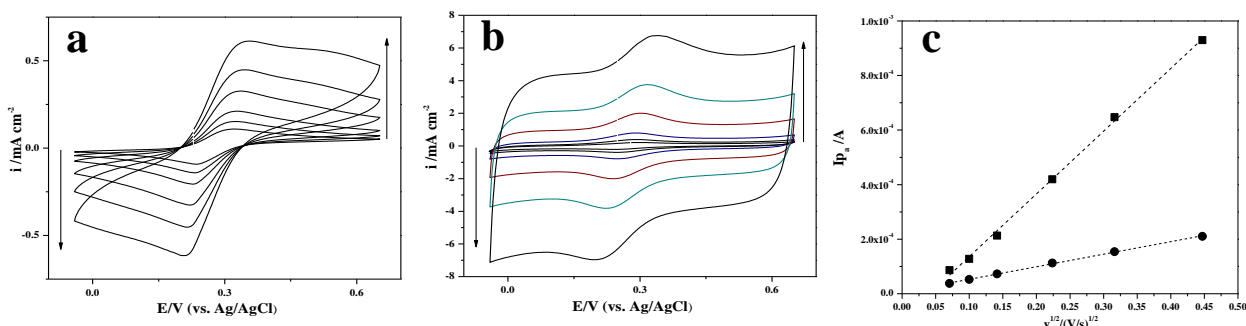


Figure 4. Cyclic voltammetry in 1 mM potassium ferrocyanide and 1 M KCl at: (a) pristine CNTs and (b) CNT_{EF}. The voltammograms were recorded with scan rates of 5, 10, 20, 50, 100 and 200 mV s⁻¹. Arrows indicate the direction of increasing scan rates. (d) Plot of the anodic peak current as function of the square root of the scan rate.

It is thus apparent that the CNT_{EF} demonstrates the fastest electron transfer kinetics. The ESA of CNT and CNT_{EF} electrodes was estimated from Fig. 4c and using the Randles–Sevcik equation [28]. An *ESA* of 0.66 cm² and 3.3 cm² were obtained for CNT and CNT_{EF}, respectively, which means that 400% more *ESA* was gained after the electrochemical functionalization process.

These results demonstrate the efficiency of the electrochemical functionalization in greatly enhancing the electron transfer properties of CNTs. Such significant enhancement in the electron transfer rate can be ascribed to the existence of large number of electroactive defects created at the surface of the CNTs that can constitute an efficient platform for enzyme immobilization.

3.3. Immobilization of GOx at CP-CNT and CP-CNT_{EF} samples

The CNTs and CNT_{EF} electrodes were soaked in phosphate buffer solution (PBS, pH=7.2) containing 15mg/mL GOx and stored overnight at 4 °C in a refrigerator. Figures 5a and 5b show SEM images taken following the GOx adsorption reaction at the surface of CNTs and CNT_{EF}, respectively. A surface-coated layer of CNTs and CNT_{EF} can be clearly differentiated from the uncoated CNT (shown in Fig. 1a) and CNT_{EF} (shown in Fig. 1b). Indeed, the surface morphology of the GOx-coated carbon nanotubes appears more coarse, although still uniform, indicating that the GOx adsorption reaction occurred homogeneously on the surface.

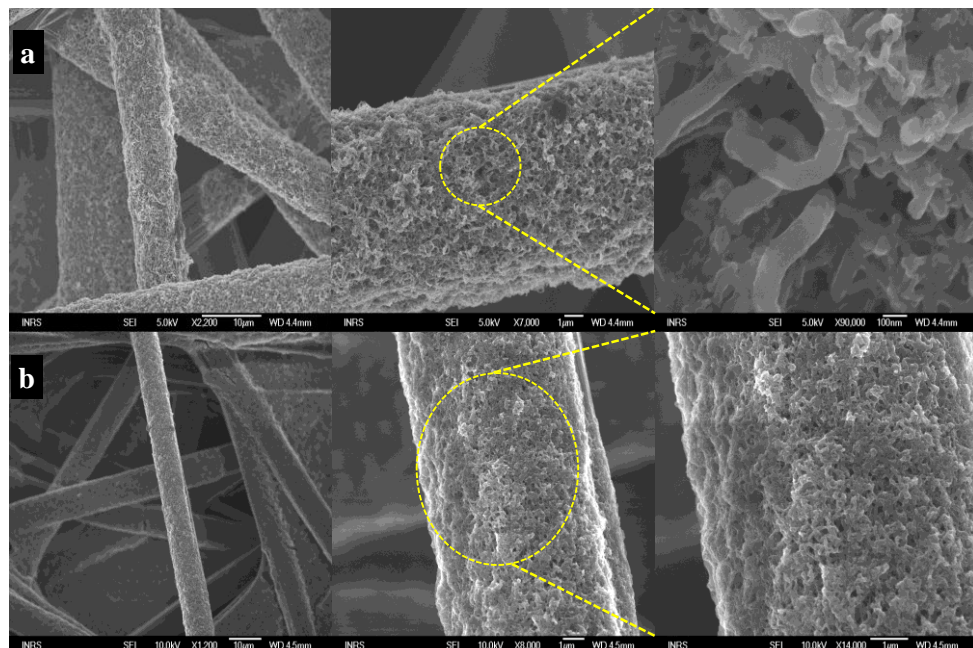


Figure 5. FESEM images with increasing magnification of: (a) CNTs coated with GOx, and (b) CNT_{EF} coated with GOx.

XPS has also proven an effective tool to quantify protein immobilized or adsorbed during enzyme immobilization [7, and references therein]. Figure 6 compares the wide survey spectra of

CNT-GOx and CNT_{EF}-GOx. Both spectra show a new element that is nitrogen with its N 1s core-level appearing at 400.5 eV. The N 1s band did not appear in XPS related to pristine CNTs and CNT_{EF} and thus can be confidently ascribed to species where nitrogen is bound to carbon and to functional groups. Thus the occurrence of nitrogen is a conclusive evidence of the GOx presence in the processed sample. The concentration of N is 7.99 and 10.55 at% at the CNT-GOx and CNT_{EF}-GOx, respectively. The N/C ratio may be an appropriate measure of the interaction of enzyme chemistry at the surface. The N/C ratio is 0.104 and 0.152 CNT-GOx and CNT_{EF}-GOx, respectively. The higher concentration of N at CNT_{EF} suggests higher degree of GOx immobilization. Exploration of the high-core levels of C 1s and O 1s after GOx immobilization showed the presence of several bands. The assignment of these bands is not easily accomplished and thus is not pursued here.

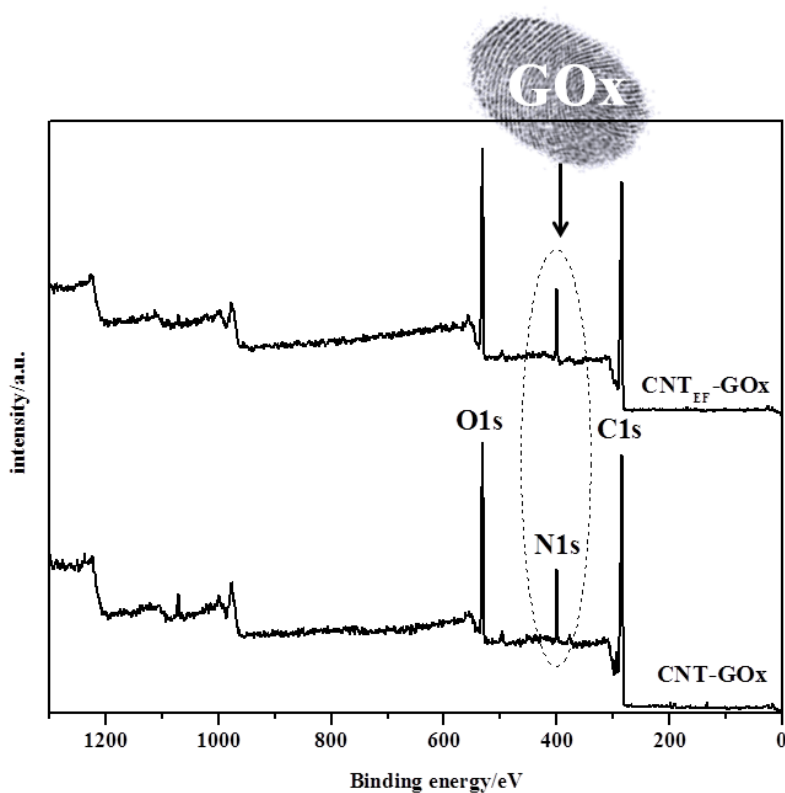


Figure 6. Wide survey XPS spectra of CNT-GOx and CNT_{EF}-GOx as labeled in the figure.

3.4. Electrochemistry at CP-CNT-GOx and CP-CNT_{EF}-GOx electrodes

Figure 7 compares CVs recorded at pristine CNT and CNT_{EF} electrodes in 0.2 M PBS at pH 7.2. It can be seen that both pristine CNTs and CNT_{EF} electrodes behave as an electrochemical double layer capacitor. The current density at the CNT_{EF} electrode is about 20 times higher than that delivered by the CNT electrode owing to the larger surface area of the former electrode.

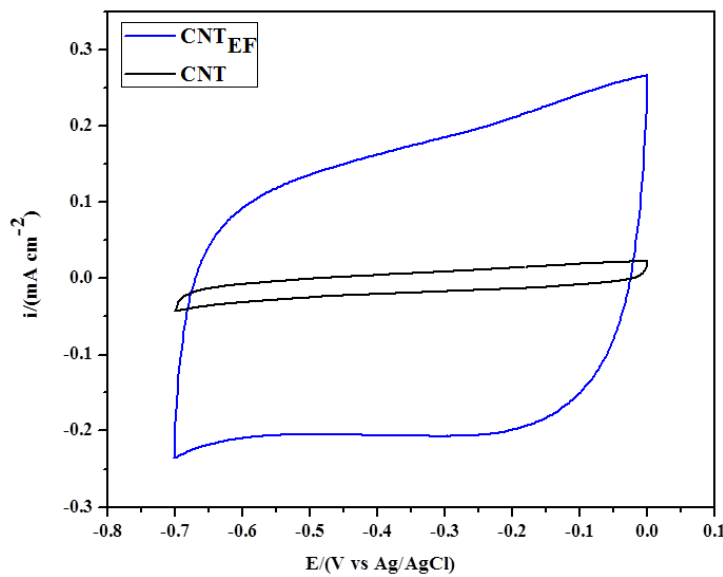


Figure 7. Cyclic voltammetry at CNT-GOx and $\text{CNT}_{\text{EF}}\text{-GOx}$ electrodes recorded at room temperature in 0.2 M PBS pH 7.2, 0.1 M KCl. Scan rate of 20 mV s^{-1} .

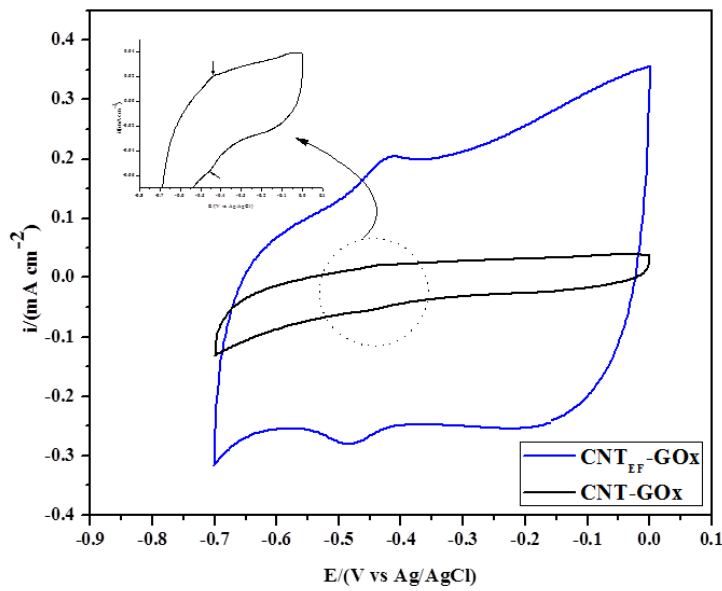
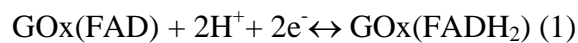


Figure 8. Cyclic voltammetry at CNT-GOx and $\text{CNT}_{\text{EF}}\text{-GOx}$ electrodes recorded at room temperature in 0.2 M PBS pH 7.2, 0.1 M KCl containing 20 mM glucose. Scan rate of 20 mV s^{-1} .

Figure 8 compares CVs recorded at pristine CNT-GOx and $\text{CNT}_{\text{EF}}\text{-GOx}$ electrodes in 20 mM glucose + 0.2 M PBS at pH 7.2, under anaerobic conditions. The current densities delivered by the

CNT-GOx are very small. However, a closer look (insert in Fig. 8) shows the presence of an oxidation (Ox) and reduction (Red) waves at -0.441 V and -0.451 V vs Ag/AgCl, respectively. On the other hand, at the CNT_{EF}-GOx electrode, the redox waves become more visible and peak shaped centered around at -0.421 V (Ox) and -0.481 V (Red) which gives a formal potential of -0.451 V. This value is very close to the FAD/FADH₂ redox potential under physiological pH [30-32]. Results shown in Fig. 8 were acquired using high concentration of glucose (20 mM) and because of the presence of large capacitive current, studying DET in low concentrated solution of glucose is not suitable with CV since the faradaic process would be difficult to distinguish owing to the presence of the high capacitive current. To study the DET with low concentrations of glucose at CNT_{EF}-GOx electrode, the SWV was employed since this technique discriminates between the capacitive current and the faradaic process [33]. Figure 9a shows SWVs recorded with an amplitude of 50 mV, a step potential of 5 mV and a frequency of 8 Hz in argon-saturated 0.2 M PBS at pH 7.2 containing various concentrations of glucose (0, 4, 10, 20, and 40 mM). Well-defined SWV peaks were obtained either in the presence of in the absence of glucose.

The SWV in the absence of glucose was conducted to clarify if GOx immobilized on CNT_{EF} surface can undergo DET with the electrode. Thus the peak observed centered at -0.407 V vs. Ag/AgCl in the absence of glucose (Fig. 9a) can be considered as a result of the redox reaction of the active site of GOx immobilized on the surface of the CP-CNT_{EF} electrode corresponding to the conversion between GOx(FAD) and GOx(FADH₂) according to Eq. (1) [34-35]:



We have conducted controlled experiment on bare CP (not coated with CNTs) and there were no peaks observed with CP/GOx electrodes (results not shown). It can be concluded that the SWV peak obtained with CP-CNT_{EF}-GOx in the absence of glucose indicates that electrical communication between the redox center of GOx and carbon paper is provided through the CNTs located on the electrode surface.

When glucose is added to the PBS solution, the peak current increased with the increase of glucose concentration up to 10 mM whereas for higher concentrations, the peak current levels off more or less (Fig. 9b). Thus, when glucose is added, the formation of FADH₂ occurs in the vicinity of the electrode surface following Eq. (2):



The increase of the current with the increase of glucose concentration demonstrates the ability of GOx to simultaneously undergo DET with the electrode and retains biocatalytic activity up to 10 mM of glucose concentration.

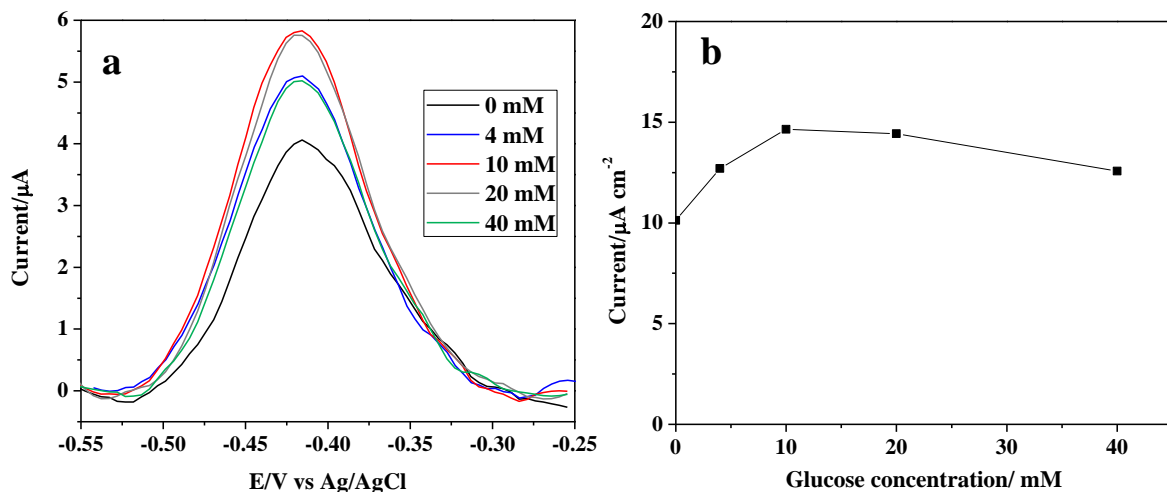


Figure 9. (a) SWVs at CNT_{EF}-GOx electrode recorded at room temperature in 0.2 M PBS pH 7.2, 0.1 M KCl containing various concentration of glucose (as indicated in the Figure). (b) Current peak density as a function of glucose concentration. The SWVs were recorded with an amplitude of 50 mV, a step potential of 5 mV and a frequency of 8 Hz.

4. CONCLUSIONS

In summary, we introduced the surface electrochemical functionalization of carbon nanotubes as an efficient approach to immobilize enzymes for biocatalytic applications in general. The electrochemical functionalization was performed by oxidizing the CNTs in a mild concentration of HNO₃ (0.2 M). This has led to an increase in the surface area and to the creation of electroactive functional groups at the surface of CNTs, which has resulted in a remarkable enhancement of their electron transfer properties.

Such large surface area and functional groups provided efficient attachment for glucose oxidase considered in this work, for instance. The GOx coating of CNTs surface was observed with SEM and further confirmed with XPS analysis.

The bioelectrocatalytic characteristics of the CP-CNT_{EF}-GOx electrodes were investigated by cyclic voltammetry and square wave voltammetry methods. The key issue was to elucidate if GOx immobilized on CP-CNT_{EF} surface can undergo DET with the electrode and, at the same time, be able to exhibit biocatalytic glucose oxidation a reaction of technological significance for biofuel cells and biosensors. The presence of an SWV redox peak in argon-saturated phosphate buffer solution (pH 7.2) in the absence of glucose was a strong indication of a DET between the GOx and the CNT_{EF}.

In presence of various concentrations of glucose, the CP-CNT_{EF}-GOx displayed bioelectrocatalytic oxidation of glucose. Indeed, the current increased with the increase of the glucose concentration up to 10 mM and saturated more or less for higher concentrations considered.

Although the concept has been presented within the context of glucose electrooxidation, it could be readily used for the immobilization and evaluation of the direct electron transfer between other enzymes or proteins and carbon nanostructures.

Further work is being carried out to investigate the ability of GOx to retain its biocatalytic activity upon long-time operation and on incorporating the CP-CNT_{EF}-GOx as an anode into a biofuel cell (under design) to examine the power density that can be issued.

ACKNOWLEDGEMENT

This work was financially supported by the Natural Sciences Engineering Research Council of Canada (NSERC), the Fonds Québécois pour la Recherche en Nature et Technologie (FQRNT), and the Centre Québécois sur les Matériaux Fonctionnels (CQMF).

References

1. A. S. Rad, A. Mirabi, E. Binaian, H. Tayebi, *Int. J. Electrochem. Sci.*, 6 (2011) 3671.
2. M. T. Meredith and S. D. Minteer, *Annu. Rev. Anal. Chem.*, 5 (2012) 157.
3. Y. Li, S.-M. Chen, R. Sarawathi, *Int. J. Electrochem. Sci.*, 6 (2011) 3776.
4. X. Wang, D. Li, T. Watanabe, Y. Shigemori, T. Mikawa, T. Okajima, L. Mao, T. Ohsaka, *Int. J. Electrochem. Sci.*, 7 (2012) 1071.
5. S. Palanisamy, S. Cheemalapati, S.-M. Chen, *Int. J. Electrochem. Sci.*, 7 (2012) 8394.
6. S. Shleev, J. Tkac, A. Christenson, T. Ruzgas, A. I. Yaropov, J. W. Whittaker and L. Gorton, *Biosens. Bioelectron.*, 20 (2005) 2517.
7. D. Ivnitski, K. Artyushkova, R. A. Rincón, P. Atanassov, H. R. Luckarift, and G. R. Johnson, *Small*, 4 (2008) 357.
8. R. P. Ramasamy, H. R. Luckarift, D. M. Ivnitski, P. B. Atanassov and G. R. Johnson, *Chem. Commun.*, 46 (2010) 6045.
9. J. Wang, M. Musameh, Y. H. Lin, *J. Am. Chem. Soc.*, 125 (2003) 2408.
10. B. Devadas, V. Mani, S.-M. Chen, *Int. J. Electrochem. Sci.*, 7 (2012) 8064.
11. S. Palanisamy, A.T. Ezhil Vilian, S.-M. Chen, *Int. J. Electrochem. Sci.*, 7 (2012) 2153.
12. A. F. Holloway, G. G. Wildgoose, R. G. Compton, L. Shao, M. L. H. Green, *J. Solid State Electrochem.*, 12 (2008) 1337.
13. S. Aquino Neto, J. C. Forti, A. R. De Andrade, *Electrocatalysis*, 1 (2010) 87.
14. E. Hao Yu and K. Scott, *Energies*, 3 (2010) 23.
15. F. Davis, S. P. J. Higson, *Biosens. Bioelectron.*, 22 (2007) 1224.
16. T. Bordjiba, M. Mohamedi, Le H. Dao, B. Aïssa, M. A. El Khakani, *Chem. Phys. Lett.*, 441 (2007) 88.
17. a) A. Tabet-Aoul and M. Mohamedi, *J. Mater. Chem.*, 22 (2011) 2491. b) A. Tabet-Aoul, F. Saidani, D. Rochefort, and M. Mohamedi *Int. J. Electrochem. Sci.*, 6 (2011) 6385.
18. M. S. Dresselhaus, G. Dresselhaus, R. Saito, A. Jorio, *Phys. Rep.*, 409 (2005) 47.
19. F. Tuinstra, and J. L. Koenig, *J. Chem. Phys.*, 53 (1970) 1126.
20. Y. Xie, P. M. A. Sherwood, *Chem. Mater.*, 2 (1990) 293.
21. N.I. Kovtyukhova, T.E. Mallouk, L. Pan, E.C. Dickey, *J. Am. Chem. Soc.*, 125 (2003) 9761.
22. J. F. Moulder, W. F. Stickle, P. E. Sobol, K. D. Bomber, *Handbook of X-ray Photoelectron Spectroscopy*, Perkin-Elmer Corporation, 1992.
23. P. M. A Sherwood, in: J. C. Riviere, S. Myhra, (Eds.), *Handbook of Surface and Interface Analysis- Methods for Problem-Solving*, Marcel Dekker: New York, 1998, pp. 605-641.
24. Yu-Qing Wang, Feng-Qiu Zhang, and Peter M. A. Sherwood, *Chem. Mater.*, 11 (1999) 2573.
25. R. Baron, F. W. Campbell, I. Streeter, L. Xiao and, R. G. Compton, *Int. J. Electrochem. Sci.*, 3 (2008) 556.
26. J. Justin Gooding, *Electrochim. Acta*, 50 (2005) 3049.
27. Craig E. Banks and Richard G. Compton, *Analyst*, 131 (2006) 15.

28. A. J. Bard, L. R. Faulkner, *Electrochemical Methods Fundamentals and Applications*, Wiley, New York, 2001.
29. R. G. Compton, C. E. Banks, *Understanding Voltammetry*, World Scientific, Singapore, 2007.
30. D. Invitski, B. Branch, P. Atanassov, C. Apblett, *Electrochem. Comm.*, 8 (2006) 1204.
31. A. Guiseppi-Elie, C. Lei, R.H. Baughman, *Nanotechnology*, 13 (2002) 559.
32. Ying Liu, Ling Liu, Shaojun Dong, *Electroanalysis*, 19 (2007) 55.
33. J. Osteryoung and J. J. O'Dea, in: A. J. Bard (Ed.), *Electroanalytical Chemistry-Square Wave Voltammetry*, vol. 14, Marcel Dekker, New York, 1986, pp. 209-303.
34. R. Ianniello, J. Lindsay, A. Yacynych, *Anal. Chem.*, 54 (1982) 1098.
35. D. Shan, J. Zhang, H.G. Xue, S.N. Ding, S. Cosnier, *Biosens. Bioelectron.*, 25 (2010) 1427.